FUSION OF ULTRASOUND AND MAGNETIC RESONANCE IMAGES FOR ENDOMETRIOSIS DIAGNOSIS: A NON-PARAMETRIC APPROACH

Youssra El Bennioui[(1)(4)], *Alexandre Bruguier*[(4)], *Fabien Vidal*[(3)], *Adrian Basarab*[(2)], *Jean-Yves Tourneret*[(1)(4)]

[(1)]Institut de Recherche en Informatique de Toulouse, CNRS UMR 5505, Université de Toulouse, France

[(2)]Univ Lyon, Université Claude Bernard Lyon 1, CNRS, Inserm, CREATIS UMR 5220, U1294, France

[(3)] Department of Gynecologic Surgery Clinique Croix Du Sud Ramsey Santé, France

[(4)] TeSA Laboratory, Toulouse, France

ABSTRACT

A fusion method was recently proposed for ultrasound and magnetic resonance images for endometriosis diagnosis. This method combined the advantages of each modality, i.e., the good contrast and signal to noise ratio of the MR image and the good spatial resolution of the US image. The method was based on an inverse problem, performing a super-resolution of the MR image and a denoising of the US image. A polynomial function was introduced to model the relationships between the gray levels of the MR and US images. This paper studies the potential interest of replacing this polynomial function by a non-parametric transformation built using the theory of reproducing kernel Hilbert spaces. Simulations conducted on a phantom and synthetic data allow the performance of the resulting fusion method to be appreciated.

Index Terms— Image fusion, MRI, ultrasound imaging, endometriosis, kernel methods, PALM.

1. INTRODUCTION

Endometriosis is a painful female disorder that takes its name from endometrium, the tissue that normally lines the uterus or the womb. It occurs when this tissue grows outside of the uterus, and becomes trapped since it cannot exit the body. It can affect the ovaries, the fallopian tubes, and other pelvic organs. More that ten percent of women are affected by endometriosis, and thus suffer severe symptoms such as painful periods and sexual intercourse, higher risk of infertility, and ovarian cancers. There is an average of 7 years for endometriosis to be diagnosed, which gives the endometrium tissue time to spread and impact several organs. Depending on the disease stage, laparoscopic surgery reveals to be the unique effective pain-relief [1].

Besides being used for diagnosis, ultrasound (US) and magnetic resonance imaging (MRI) are used to identify the endometrial implant and its depth of infiltration in organs before surgery. MR and US images are two different imaging modalities that differ by the technologies behind them and therefore offer several advantages and limitations. US imaging is a modality with a high spatial resolution that provides fine internal details of a structure. However, this modality has some limitations including a limited field of view and low signal to noise ratio. On the other hand, MRI offers a wide field of view of patient anatomy with a good signal to noise ratio but with a relatively low spatial resolution. Hence, precise anatomic landmarks at the millimetric scale may be under-evaluated when using this modality alone. In order to combine their complementary properties, MRI and US are classically used separately for clinical analysis and medical intervention.

Image fusion refers to assembling all the important information from multiple images and including them in fewer images, e.g., in a single image. The purpose of image fusion is to build an enhanced image that is informative, comprehensible and accurate for the desired application. Image fusion is common in medical imaging and generally allows better decisions in clinical studies. Medical images that can be fused efficiently include MR and single-photon emission computed tomography (SPECT) images [2], MRI and computed tomography (CT) [3], or positron emission tomography (PET) and CT [4]. A US-MR image fusion algorithm was recently proposed to create a hybrid image (referred to as MAR-IUS image, for MAgnetic Resonance Imaging & UltraSound) gathering the advantages of both modalities in the context of endometriosis diagnosis [5]. The MARIUS image resulting from this algorithm was shown to have a spatial resolution comparable to the US image and an SNR and contrast close to the MR image. Note that this algorithm requires registered 2D US and 3D MR images, which can be performed using the method studied in [6].

The idea developed in [5] was to build two observation models associated with US and MR images to exploit the complementarity of both images in terms of resolution and contrast. A linear model formed by blurring and downsampling operators was proposed for the MR image, motivated by its good performance for super-resolution [7–9]. A denoising model was considered for the US image in order to mitigate the effect of speckle noise [10, 11]. Since US and MR modalities are different by their nature and content, there is no simple correspondence between the gray levels of these images. Motivated by [12], a polynomial transformation was used in [5] to link the intensities of these modalities. The objective of this paper is to study the relevance of replacing this polynomial

by a non-parametric transformation defined using the theory of reproducing kernels. These methods have been used successfully in the context of point cloud registration [13], image denoising [14], super-resolution [15] and segmentation [16]. This paper studies their interest for image fusion by incorporating them into the fusion model of [5] and estimating the MARIUS image using a proximal alternating linearized minimization (PALM) algorithm [17]. The proposed fusion method is evaluated on an experimental phantom and realistic data generated from an in vivo MRI volume, with a specific attention to endometriosis treatment.

The remainder of the paper is organized as follows. Section 2 briefly summarizes the fusion algorithm presented in [5] using a polynomial function. The proposed fusion algorithm based on a non parametric transformation between US and MR images is studied in Section 3. Experiments are presented and discussed in Section 4. Conclusions and perspectives are finally reported in Section 5.

2. FUSION USING A POLYNOMIAL FUNCTION

The following observation models were considered in [5]:

$$
\begin{aligned}
\boldsymbol{y}_{\mathrm{mri}} &= \boldsymbol{SC}\boldsymbol{x}_{\mathrm{mri}} + \boldsymbol{n}_m, \\
\boldsymbol{y}_{\mathrm{us}} &= \boldsymbol{x}_{\mathrm{us}} + \boldsymbol{n}_u,
\end{aligned}
\tag{1}
$$

where $\boldsymbol{x}_{\mathrm{mri}} \in \mathbb{R}^N$ is the non-observable high-resolution vectorized MR image, $\boldsymbol{y}_{\mathrm{mri}} \in \mathbb{R}^M$ is the low-resolution observed MR image, $\boldsymbol{n}_m \in \mathbb{R}^N$ is an independent identically distributed (i.i.d.) additive white Gaussian noise with variance σ_m^2, $\boldsymbol{C} \in \mathbb{R}^{N \times N}$ is a matrix with block circulant with circulant blocks modelling the blurring effect of the MRI point spread function (PSF) with circulant boundary conditions, $\boldsymbol{S} \in \mathbb{R}^{M \times N}$ (with $N = d_m^2$) is a decimation operator with a decimation factor d. On the other hand, $\boldsymbol{y}_{\mathrm{us}} \in \mathbb{R}^N$ is the vectorized observed B-mode US image, $\boldsymbol{x}_{\mathrm{us}} \in \mathbb{R}^N$ is the vectorized speckle noise-free US image and $n_u \in \mathbb{R}^N$ is an i.i.d. log-Rayleigh noise sequence with localization parameter γ. A polynomial was used in [5] to link $\boldsymbol{x}_{\mathrm{us}}$ and $\boldsymbol{x}_{\mathrm{mri}}$:

$$
\boldsymbol{x}_{\mathrm{us}} = f\left(\boldsymbol{x}_{\mathrm{mri}}, \nabla \boldsymbol{x}_{\mathrm{mri}}^H \boldsymbol{u}\right),
\tag{2}
$$

where $f : \mathbb{R}^N \times \mathbb{R}^N \to \mathbb{R}^N$ is an unknown polynomial function of the image $\boldsymbol{x}_{\mathrm{mri}}$, its gradient, and the US scan direction $\boldsymbol{u}$. This function will be denoted as $\phi\left(\boldsymbol{x}, \boldsymbol{u}\right) = f\left(\boldsymbol{x}, \nabla \boldsymbol{x}^H \boldsymbol{u}\right)$ for brevity. This leads to the following optimization problem:

$$
\hat{\mathbf{x}} = \underset{\mathbf{x}}{\operatorname{argmin}} \underbrace{\frac{1}{2}\|\boldsymbol{y}_{\mathrm{mri}} - \boldsymbol{SC}\mathbf{x}\|^2}_{\text{MRI data fidelity}} + \underbrace{\tau_1\|\nabla \mathbf{x}\|^2 + \tau_3\|\nabla \phi(\mathbf{x}, \boldsymbol{u})\|^2}_{\text{regularization}}
$$

$$
+ \underbrace{\tau_2 \sum_{i=1}^{N} \left\{ \exp\left[\boldsymbol{y}_{\mathrm{us},i} - \phi_i(\boldsymbol{x}, \boldsymbol{u})\right] - \gamma \exp\left[\boldsymbol{y}_{\mathrm{us},i} - \phi_i(\boldsymbol{x}, \boldsymbol{u})\right] \right\}}_{\text{US data fidelity}}
$$

that can be solved using the proximal alternating linearized minimization (PALM) [5].

3. FUSION USING REPRODUCING KERNELS

This section defines a new function f to link US and MR images based on reproducing kernels. Kernel methods have become universal since they are capable of approaching complex non linear relationships between signal and images. They need to define an appropriate kernel function between the signals or images of interest such as the Gaussian kernel with parameter β defined as:

$$
K(\boldsymbol{x}, \boldsymbol{y}) = \exp\left(-\beta\|\boldsymbol{x} - \boldsymbol{y}\|^2\right),
\tag{3}
$$

where $\|.\|$ is an appropriate norm. In this paper, as in [14], $\boldsymbol{x}$ and $\boldsymbol{y}$ are patches of size $n \times n$ centered around pixels of the US and MR images. The idea is that each pixel of a patch in the noise-free US image is a linear combination of the kernel applied to the pixels of the corresponding MR image patch. Since a given pixel of the US image belongs to several patches, the final value of the pixel intensity of the US image is the average of the intensities resulting from different patches, i.e.,

$$
\boldsymbol{x}_{\mathrm{us},i} = \frac{1}{n_i} \sum_{p \in J_i} \left[\sum_{k=1}^{n^2} c_{p,k} K(\boldsymbol{x}_{\mathrm{mri},i}, \boldsymbol{x}_{\mathrm{mri},h_k(p)}) \right],
\tag{4}
$$

where $\boldsymbol{x}_{\mathrm{us},i}$ is the ith US pixel (belonging to different patches of size n^2), J_i is the set of indices of the patches containing the pixel i, $n_i \leq n^2$ is the cardinality of J_i (each patch is identified by the index of its central pixel) and $h_k(p)$ is the index of the kth pixel of Patch $\#p$. To estimate the coefficient vector $\boldsymbol{c}_p = (c_{p,1}, ..., c_{p,n^2})^T$ of Patch $\#p$, we assume that the transformation (4) is also valid for the observed MR and US images and consider the least squares (LS) estimator[1]:

$$
\min_{\boldsymbol{c}_p} \sum_{i=1}^{n^2} \left[\boldsymbol{y}_{\mathrm{us},i} - \sum_{k=1}^{n^2} c_{p,k} K(\boldsymbol{y}_{\mathrm{mri},i}, \boldsymbol{y}_{\mathrm{mri},h_k(p)}) \right]^2,
\tag{5}
$$

that can be written in matrix form as:

$$
\min_{\boldsymbol{c}_p} ||\boldsymbol{A}\boldsymbol{c}_p - \boldsymbol{p}_{\mathrm{us}}||^2,
\tag{6}
$$

where $A_{i,j} = K(\boldsymbol{p}_{\mathrm{mri}_i}, \boldsymbol{p}_{\mathrm{mri}_j})$, $\boldsymbol{p}_{\mathrm{us}}$ and $\boldsymbol{p}_{\mathrm{mri}}$ are patches extracted from $\boldsymbol{y}_{\mathrm{us}}$ and $\boldsymbol{y}_{\mathrm{mri}}$. The solution of (6) is $\hat{\boldsymbol{c}}_p = \boldsymbol{A}^\dagger \boldsymbol{p}_{\mathrm{us}}$, where $\boldsymbol{A}^\dagger = (\boldsymbol{A}^T \boldsymbol{A})^{-1} \boldsymbol{A}^T$ is the pseudo-inverse of $\boldsymbol{A}$.

3.1. PALM Algorithm

This section studies a PALM algorithm allowing (1) to be solved, when the US and MR images are linked by (4). We

---

[1]Another strategy would be to plug the relation (4) into the observation models (1) and to estimate jointly the unknown image $\boldsymbol{x}_{\mathrm{mri}}$ and the coefficient vector $\boldsymbol{c}_p$ using a modified PALM algorithm.

introduce the following functions:

$$l(\boldsymbol{x}) = \frac{1}{2}||\boldsymbol{y}_{\text{mri}} - \boldsymbol{SCx}||^2 + \tau_1||\nabla\boldsymbol{x}||^2$$

$$g(\boldsymbol{v}) = \tau_2 \sum_{i=1}^{N} \left[\exp(\boldsymbol{y}_{\text{us},i} - \boldsymbol{v}_i) - \gamma(\boldsymbol{y}_{\text{us},i} - \boldsymbol{v_i})\right] + \tau_3||\nabla\boldsymbol{v}||^2$$

$$H(\boldsymbol{x}, \boldsymbol{v}) = \tau_4 \sum_{i=1}^{N} \left(\boldsymbol{v}_i - \frac{1}{n_i} \sum_{p \in J_i} \left[\sum_{k=1}^{n^2} c_{p,k} K(\boldsymbol{x}_i, \boldsymbol{x}_{h_k(p)})\right]\right)$$

which differ from [5] only by the definition of H, which involves kernel functions instead of polynomials. Note that l and g include data fidelity terms associated with the MR and US images and that H is used to enforce the relationship between the US and MR images based on kernels (defined in (4)). Using these definitions, the PALM algorithm reduces to alternate between updates of and $\boldsymbol{x}$ and $\boldsymbol{v}$ as explained below.

3.1.1. Update x

The first step of PALM algorithm reduces to

$$\boldsymbol{x}^{k+1} = \text{prox}_{L_{k+1}}^{l} \left(\boldsymbol{x}^k - \frac{1}{L_{k+1}}\nabla_{\boldsymbol{x}}H(\boldsymbol{x}^k, \boldsymbol{v}^k)\right),$$

$$= \text{argmin}_{\boldsymbol{x}} \left\{ \frac{1}{2}||\boldsymbol{SCx} - \boldsymbol{y}_m||^2 + \tau_1||\nabla\boldsymbol{x}||^2 \right.$$

$$\left. + \frac{L_{k+1}}{2} \left\|\boldsymbol{x} - \left(\boldsymbol{x}^k - \frac{1}{L_{k+1}}\nabla_{\boldsymbol{x}}H(\boldsymbol{x}^k, \boldsymbol{v}^k)\right)\right\|^2 \right\},$$

with L_{k+1} the Lipschitz constant at iteration $k + 1$ given in [5]. This minimization problem admits an analytical solution, which can be computed efficiently in the Fourier domain. The update of $\boldsymbol{x}$ at iteration $k + 1$ is obtained as follows:

$$\boldsymbol{x}^{k+1} = \left[\boldsymbol{C}^H\boldsymbol{S}^H\boldsymbol{SC} + 2\left(\tau_1\boldsymbol{D} + \frac{L_{k+1}}{2}\boldsymbol{I}_N\right)\right]^{-1}\boldsymbol{R}, \quad (7)$$

with $\boldsymbol{D} = \boldsymbol{D}_h^H\boldsymbol{D}_h + \boldsymbol{D}_v^H\boldsymbol{D}_v$ and

$$\boldsymbol{R} = \boldsymbol{C}^H\boldsymbol{S}^H\boldsymbol{y}_{\text{mri}} + 2L_{k+1}\left[\boldsymbol{x}^k - \frac{1}{L_{k+1}}\frac{2\beta\tau_4}{\boldsymbol{n}}\right.$$

$$\left. \times \sum_{p \in J}\sum_{k=1}^{n^2} c_{p,k}(\boldsymbol{x}^k - \boldsymbol{x}_{h_k(p)})K(\boldsymbol{x}^k, \boldsymbol{x}_{h_k(p)})\right],$$

where $\boldsymbol{D}_h$ and $\boldsymbol{D}_v$ are the horizontal and vertical finite difference operators, $\boldsymbol{n} = (n_1, ..., n_N)^T$ and $\boldsymbol{J} = (J_1, ..., J_N)^T$ gathers all the patches. The direct computation of (7) requires the inversion of a high-dimensional matrix, which can be handled using a diagonalization in the Fourier domain [5].

3.1.2. Update v

The vector $\boldsymbol{v}$ is updated by computing the proximal PALM operator by gradient descent, given that the function to be

minimized here is differentiable and convex, i.e.,

$$\boldsymbol{v}^{k+1} = \text{argmin}_{\boldsymbol{v}} \quad \tau_2 \sum_i [\exp(y_{\text{us},i} - v_i) - \gamma(y_{\text{us},i} - v_i)] +$$

$$\tau_3||\nabla\boldsymbol{v}||^2 + \frac{d_k}{2}\left\|\boldsymbol{v} - \left(\boldsymbol{v}^k - \frac{1}{d_k}\nabla_{\boldsymbol{v}}H(\boldsymbol{x}^{k+1}, \boldsymbol{v}^k)\right)\right\|^2,$$

$$(8)$$

with $d_k = L_{\boldsymbol{v}}(\boldsymbol{x}^k) = 2\tau_4$ the Lipschitz constant of $\nabla_{\boldsymbol{v}}H$.

3.1.3. Proposed fusion algorithm

Algorithm 1 summarizes the different steps of the proposed fusion algorithm using reproducing kernels:

> **Input** : $\boldsymbol{y}_m, \boldsymbol{y}_u, \boldsymbol{S}, \boldsymbol{C}, \tau, \gamma, \beta$
> Estimate the coefficients of the kernel as $\hat{\boldsymbol{c}}_p = \boldsymbol{A}^\dagger\boldsymbol{p}_{\text{us}}$;
> **while** *stopping criterion is not satisfied* **do**
>   **Step 1 :** Compute L_{k+1} as in [5] and update $\boldsymbol{x}$
>   using (7);
>   **Step 2 :** Set $d_k = 2\tau_4$ and update $\boldsymbol{v}$ using (8);
> **end**
> **Output:** Fused image $\boldsymbol{x}$

Algorithm 1: Proposed Kernel-based Fusion Algorithm.

4. EXPERIMENTS

4.1. Synthetic data from real MR acquisition

The proposed MRI/US fusion algorithm was first validated on synthetic data. The simulations presented hereafter have been obtained using a real high resolution MR image that has been degraded to generate an image close to that obtained for endometriosis surgery. The 3D high resolution MR volume corresponds to a real pelvic MRI capturing the uterus, bladder and endometriosis lesions. A blurred and noisy 3D MRI is then generated from this high-resolution MR volume. More precisely, the HR volume was blurred using a 2D Gaussian filter of standard deviation $\sigma^2 = 4$, and then was contaminated by an additive white Gaussian noise (SNR = 21.5 dB), yielding the MR image displayed in Fig. 1(a). A kernel transformation as defined in (4) was used to generate the clean US image from the corresponding clean high-resolution MR image. Then, log-Rayleigh additive noise was added, yielding the image displayed in Fig. 1(b) (SNR= 11.5 dB).

The performance of the fusion method was evaluated qualitatively through visual inspection of the final image, and quantitatively using the contrast-to-noise ratio (CNR). For two patches extracted from two different structures (uterus and bladder in this case), the CNR is defined as CNR $= \frac{|\mu_i - \mu_j|}{\sqrt{\sigma_i^2 + \sigma_j^2}}$, where $\mu_i, \mu_j, \sigma_i^2, \sigma_j^2$ are the means and standard deviations of two blocks of pixels.

The MARIUS image obtained using the proposed algorithm is displayed in Fig. 1(c). This image provides a good compromise between the US and MR data. Specifically, the fused
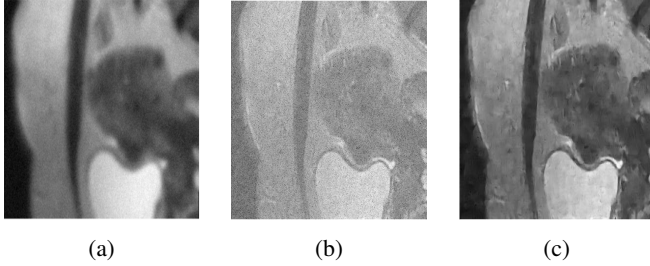
Fig. 1: (a) MR image, (b) US image, (c) MARIUS image.

image is less affected by US speckle and MRI blur, provides well-defined contours and good contrast compared to the native MR and US images. The CNR values for the MR and the US images are 39.52 dB and 27.15 dB, whereas the MARIUS images obtained using polynomial and kernel transformations have CNRs equal to 34.96 dB and 38.65 dB. These results show the interest of replacing the polynomial by a kernel.

4.2. Phantom data

This section evaluates the proposed fusion algorithm on experimental phantom data. The phantom was made of a beaf steak on top of which was stuck a polyvinyl alcohol (PVA) phantom using cyanoacrylate instant glue. It was designed to mimic uterus and endometrium responses to MR and US imaging. More details about the experimental model design and image acquisition can be found in [18]. The sizes of the acquired images are (600×600) for the US, and $(320 \times 320 \times 90)$ for the MRI volume. The field of view of the MR image is wider than the one of the US image. Therefore, the MR volume was manually cropped to $(100 \times 100 \times 90)$ to ensure similar fields of view for the two modalities. Bicubic interpolation of the MR image was finally performed to ensure the same pixel size in MR and US images. Note that the proposed fusion method requires registered images obtained using the algorithm of [6] and shown in Figs. 2(a,b).
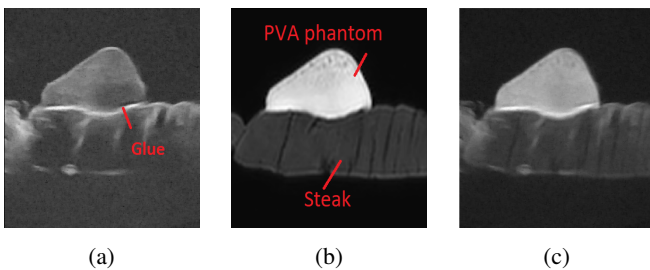
Fig. 2: (a) US image, (b) MR image, (c) MARIUS image.

The proposed fusion algorithm was applied to the US and MR images with the following parameters: $\beta = 10^{-5}, \tau_1 = 10^{-5}, \tau_2 = 0.5, \tau_3 = 0.01$ and $\tau_4 = 10^{-5}$, which were determined by cross validation. The first result is that the fused image shown in Fig. 2(c) has a good spatial resolution sim-

ilar to the US image, and a contrast equivalent to the MRI. In particular, the different structures of interest are much better highlighted: (i) the glue between the steak and the PVA phantom, mimicking the depth of penetration, not visible on MRI because of the lack of resolution, appears clearly on the US and MARIUS images; (ii) the steak and the PVA are well contrasted on the MR and MARIUS images, which is not the case in the US image.

Fig. 3 shows image profiles extracted from the US, MR and MARIUS images using a kernel transformation (proposed method) and a polynomial [5]. The interest of fusing MR and US images is clear, with more pronounced edges with the proposed kernel method. Quantitivative results are provided in Tab. 1, which reports the CNR values between the PVA phantom and the beef steak for the different images.
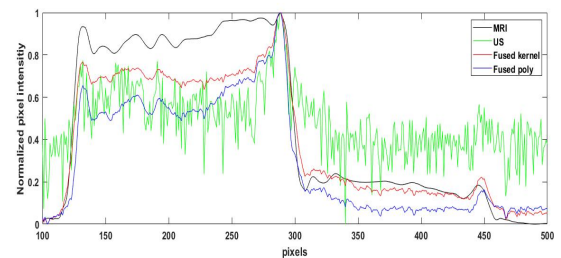
Fig. 3: Normalized pixel intensities of US, MRI, and MARIUS images using polynomial and kernel functions.

	MRI	US	Fused kernel	Fused poly
CNR	54.21 dB	32.37 dB	52.23 dB	43.17 dB

Table 1: CNR values for the US, MR and MARIUS images.

5. CONCLUSION

This paper studied a new fusion method based on reproducing kernels for MR and US images. The fused MARIUS image obtained with this method brings together the advantages of both modalities: resolution and contrast. However, the MARIUS image is more contrasted when using a kernel transformation instead of a polynomial. This improved contrast is clearly interesting for the detection and treatment of lesions related to endometriosis. Another significant advantage in favour of the kernel transformation is that it is not directly related to the direction of propagation of the scan US (vector $\boldsymbol{u}$ in [5]), which is not easy to obtain in practical applications. The price to pay with the proposed approach is its computational complexity. Indeed, unlike the polynomial approach which requires only about ten coefficients to be estimated upstream, the kernel transformation may need some hundreds of thousands of parameters to be estimated depending on the image and patch sizes. Future work will be devoted to including the MARIUS image into an augmented reality system for endometriosis surgery.

6. REFERENCES

[1] T. Z. Jacobson, J. Mn Duffy, D. Barlow, C. Farquhar, P. Koninckx, and D. Olive, "Laparoscopic surgery for subfertility associated with endometriosis," *Cochrane Database of Systematic Reviews*, vol. 1, 2010.

[2] U. Pietrzyk, K. Herholz, A. Schuster, H.-M. Stock-hausen, H. Lucht, and W.-D. Heiss, "Clinical applications of registration and fusion of multimodality brain images from PET, SPECT, CT, and MRI," *European journal of radiology*, vol. 21, no. 3, pp. 174–182, 1996.

[3] A. Wong and W. Bishop, "Efficient least squares fusion of MRI and CT images using a phase congruency model," *Pattern Recognition Letters*, vol. 29, no. 3, pp. 173–180, 2008.

[4] W. Vogel V, W. Oyen, J. Barentsz, J. Kaanders, and F. Corstens, "PET/CT: panacea, redundancy, or something in between?," *Journal of Nuclear Medicine*, vol. 45, no. 1, pp. 15S, 2004.

[5] O. El Mansouri, F. Vidal, A. Basarab, P. Payoux, D. Kouamé, and J.-Y. Tourneret, "Fusion of Magnetic Resonance and Ultrasound images for endometriosis detection," *IEEE Trans. Image Process.*, vol. 29, pp. 5324–5335, 2020.

[6] Y. El Bennioui, F. Vidal, A. Basarab, and J.-Y. Tourneret, "Joint registration and fusion of 3D Magnetic resonance and 2D Ultrasound images for endometriosis surgery," in *Proc. European Signal Processing Conference (EUSIPCO)*, Helsinki, Finland, 2023.

[7] A. Gholipour, J. A. Estroff, and S. K. Warfield, "Robust super-resolution volume reconstruction from slice acquisitions: application to fetal brain MRI," *IEEE Trans. Med. Imag.*, vol. 29, no. 10, pp. 1739–1758, 2010.

[8] H. Greenspan, G. Oz, N. Kiryati, and S. Peled, "MRI inter-slice reconstruction using super-resolution," *Magnetic resonance imaging*, vol. 20, no. 5, pp. 437–446, 2002.

[9] J. V. Manjón, P. Coupé, Antonio A. Buades, D. L. Collins, and M. Robles, "MRI superresolution using self-similarity and image priors," *International journal of biomedical imaging*, vol. 2010, 2010.

[10] T. Aysal and K. E. Barner, "Rayleigh-maximum-likelihood filtering for speckle reduction of ultrasound images," *IEEE Trans. Med. Imag.*, vol. 26, no. 5, pp. 712–727, 2007.

[11] S. Gupta, R. C. Chauhan, and S. C. Saxena, "Locally adaptive wavelet domain bayesian processor for denoising medical ultrasound images using speckle modelling based on Rayleigh distribution," *Proc. Vis. Image Signal Process.*, vol. 152, no. 1, pp. 129–135, 2005.

[12] A. Roche, X.Pennec, G. Malandain, and N. Ayache, "Rigid registration of 3D ultrasound with MR images: a new approach combining intensity and gradient information," *IEEE Trans. Med. Imag.*, vol. 20, no. 10, pp. 1038–1049, 2001.

[13] J. Ma, J. Zhao, and A. L. Yuille, "Non-rigid point set registration by preserving global and local structures," *IEEE Trans. Image Process.*, vol. 25, no. 1, pp. 53–64, January 2016.

[14] P. Bouboulis, K. Slavakis, and S. Theodoridis, "Adaptative kernel-based image denoising employing semi-parametric regularization," *IEEE Trans. Image Process.*, vol. 19, no. 1, pp. 1465–79, 2010.

[15] L.-J. Deng, W. Guo, and T.-Z. Huang, "Single-image super-resolution via an iterative reproducing kernel hilbert space method," *IEEE Trans. Circuits Syst. Video Technol.*, vol. 26, no. 11, pp. 2001–2014, 2016.

[16] S. H. Kang, B. Shafei, and G. Steidl, "Supervised and transductive multi-class segmentation using p-laplacians and RKHS methods," *Journal of Visual Communication and Image Representation*, vol. 25, no. 5, pp. 1136–1148, 2014.

[17] J. Bolte, S. Shoham, and M. Teboulle, "Proximal alternating linearized minimization or nonconvex and nonsmooth problems," *Mathematical Programming*, vol. 146, no. 1-2, pp. 459–494, 2014.

[18] F. Vidal, O. El Mansouri, D. Kouamé, and A. Basarab, "On the design of a pelvic phantom for Magnetic Resonance and Ultrasound image fusion," in *Proc. IEEE IUS Symp.*, Glasgow, UK, 2019, pp. 2400–2403.